

New Approaches to Modeling Failure and Fracture of Rubberlike Materials



K. Y. Volokh

Contents

- 1 Introduction
 - 2 Failure as Onset of Damage
 - 2.1 Elasticity with Energy Limiters
 - 2.2 Cavitation
 - 2.3 Strength of Soft Composites
 - 2.4 Prediction of Crack Direction
 - 3 Fracture as Damage Localization
 - 3.1 Material Sink Formulation
 - 3.2 Dynamic Crack Propagation
 - 4 Final Remarks
- References

Abstract In this chapter we review some recent approaches to modeling failure and fracture of soft materials. By failure we mean the onset of damage via material instability. By fracture we mean further localization of damage into cracks with their subsequent propagation.

Mathematical description of failure is simple and it only requires some bounding of the strain energy density. The bounded strain energy automatically implies the bounded achievable stress, which is an indicator of material failure. By bounding the strain energy via energy limiters we show, for instance, how to explain cavitation, analyze strength of soft composites, and predict direction of possible cracks.

Mathematical description of fracture is more involved because it requires regularized formulations suppressing the so-called pathological mesh sensitivity. Most existing approaches utilize purely formal regularization schemes that lack physical grounds. We discuss a more physically based approach rooted in the idea that bulk

K. Y. Volokh (✉)

Faculty of Civil and Environmental Engineering, Technion – Israel Institute of Technology,
Haifa, Israel

e-mail: cvolokh@technion.ac.il

cracks are not a peaceful unzipping of adjacent atomic layers but rather a catastrophic explosion of bonds localized within a finite characteristic area.

1 Introduction

Failure and fracture are the central unsolved problems in solid mechanics generally and in mechanics of soft materials particularly. In this chapter we present some recent developments towards the solution of the problem. We emphasize the distinction between the concept of failure, which we interpret as the onset of material instability and damage, and the concept of fracture, which we interpret as the localization of damage into cracks and their dynamic propagation. We strongly believe that the only consistent description of failure and fracture should be the one incorporated in constitutive equations. For the general theoretical background and notation we refer to [1].

2 Failure as Onset of Damage

Traditional strength-of-materials approach defines material strength as the maximum stress achievable in uniaxial tension experiments. Various other criteria can be imposed on stresses or strains to define the state of failure. Importantly, such criteria are not a part of the constitutive laws. Rather, they are extra conditions or constraints that should be obeyed in analysis and design in order to provide reliable mechanical behavior of materials and structures. The strength-of-materials approach is seemingly simple yet it can be dangerous. For example, the critical strains of highly stretchable elastomers are much lower in equibiaxial as compared to uniaxial tension. Thus, the criterion of the critical uniaxial stretches is not applicable to structures under biaxial deformation. The latter notion is not always appreciated and understood by designers.

More convincing would be a description of failure which is directly incorporated in the constitutive law. In the latter case, there is no need to search for and obey extra constraints and the onset of failure naturally comes out of the stress analysis. We note that the traditional constitutive laws for elastomers do not describe failure: numerous hyperelastic models describe the intact mechanical behavior of materials. Moreover, various restrictions (e.g. poly-convexity, strong ellipticity, Baker–Ericksen inequalities, etc. [2]) are usually imposed on the hyperelastic constitutive laws in order to provide material stability. Such restrictions preclude from a description of material failure. Obviously, that is not physical because all materials fail.

To describe material failure the approach of continuum damage mechanics (CDM) was developed in which a damage variable was used [3–12]. The damage variable is an internal parameter whose physical meaning is open to debate.

Mathematically, the internal variable is utilized to reduce material stiffness during the damage process. The additional variable requires extra evolution equation and a threshold condition for its activation. This approach is especially appealing when the accumulation of damage is gradual. In the case of the abrupt damage a simpler approach is available [13] which does not require any internal variables. The latter approach of energy limiters and its implications are considered below.

2.1 Elasticity with Energy Limiters

We assume that the local deformation of material is described by the deformation gradient: $\mathbf{F} = \text{Grady} = \partial \mathbf{y} / \partial \mathbf{x}$; where $\mathbf{x} \in \Omega_0$ and $\mathbf{y}(\mathbf{x}) \in \Omega$ denote the referential and current positions of a generic material point accordingly. The linear and angular momenta balance and the hyperelastic constitutive law read

$$\rho_0 \ddot{\mathbf{y}} = \text{Div} \mathbf{P}, \quad \mathbf{P} \mathbf{F}^T = \mathbf{F} \mathbf{P}^T, \quad \mathbf{P} = \partial \psi / \partial \mathbf{F}, \quad (1)$$

where ρ_0 is the referential mass density; $\ddot{\mathbf{y}}$ is the acceleration; \mathbf{P} is the first Piola–Kirchhoff stress tensor; $(\text{Div} \mathbf{P})_i = \partial P_{ij} / \partial x_j$; and ψ is the strain energy density.

The corresponding natural boundary condition expresses this same linear momentum balance law on the boundary $\partial \Omega_0$,

$$\mathbf{P} \mathbf{n}_0 = \bar{\mathbf{t}}_0, \quad (2)$$

where $\bar{\mathbf{t}}_0$ is the given surface traction and \mathbf{n}_0 is a unit outward normal to $\partial \Omega_0$.

Alternatively to (2), essential boundary conditions for placements can be prescribed on $\partial \Omega_0$

$$\mathbf{y} = \bar{\mathbf{y}}. \quad (3)$$

In addition, initial conditions in Ω_0 complete the formulation of the problem

$$\mathbf{y}(t = 0) = \mathbf{y}_0, \quad \dot{\mathbf{y}}(t = 0) = \mathbf{v}_0. \quad (4)$$

We note again that a traditional strain energy function describes material that never fails. Such a description directly contradicts reality. Indeed, the number of atoms/molecules is limited within any material volume and, consequently, their bond energy is limited. The latter notion implies that the macroscopic strain energy density must also be limited. We emphasize that the latter conclusion is a direct consequence of the structure of matter. Introduction of the limited strain energy is not a matter of choice – it is a physics demand.

Table 1 Material constants

c_1 [MPa]	c_2 [MPa]	c_3 [MPa]	Φ [MPa]	m
0.298	0.014	0.00016	82.0	10

One can imagine various ways to introduce the limited strain energy. We use the upper incomplete gamma function, $\Gamma[s, x] = \int_x^\infty t^{s-1} e^{-t} dt$, for the following definition of the generic bounded strain energy density [14, 15]

$$\psi(\mathbf{F}) = \psi_f - \psi_e(\mathbf{F}), \quad (5)$$

where

$$\psi_e(\mathbf{F}) = \Phi m^{-1} \Gamma[m^{-1}, W(\mathbf{F})^m \Phi^{-m}], \quad \psi_f = \psi_e(\mathbf{1}). \quad (6)$$

Here, we designated failure energy by ψ_f ; elastic energy by $\psi_e(\mathbf{F})$; strain energy without failure by $W(\mathbf{F})$; the energy limiter (average bond energy) by Φ ; identity tensor by $\mathbf{1}$; and material parameter by m .

We note that the increase of deformation beyond some critical threshold will lead to the decrease of the elastic energy: $\psi_e \rightarrow 0$, which will numerically vanish. In this case, the strain energy will approach the failure energy: $\psi \rightarrow \psi_f$, indicating a fixed energy dissipation. To make the process irreversible it is possible to slightly modify (5) – see [16]. However, the irreversibility is important when damage localization is considered and we postpone its discussion to the section on fracture.

Substitution of (5) in (1)₃ yields a simple form of the constitutive law

$$\mathbf{P} = \exp[-W^m \Phi^{-m}] \partial W / \partial \mathbf{F}. \quad (7)$$

Remarkably, the latter constitutive equation does not include any gamma function and only the exponential factor makes difference between the present formulation and traditional hyperelasticity with the intact material behavior. The exponential term has two major modes. It equals one for the intact material behavior and it goes to zero for damage. The subtle transition between these two modes provides a description of the onset of failure.

By way of illustration, we specify the intact strain energy for natural rubber as follows [15]:

$$W = c_1(I_1 - 3) + c_2(I_1 - 3)^2 + c_3(I_1 - 3)^3, \quad (8)$$

where $I_1 = \mathbf{F} : \mathbf{F}$ is the first principal invariant and material is incompressible: $J = \det \mathbf{F} = 1$.

Material constants were fitted [15] to the experimental data from [17] and they are given in Table 1.

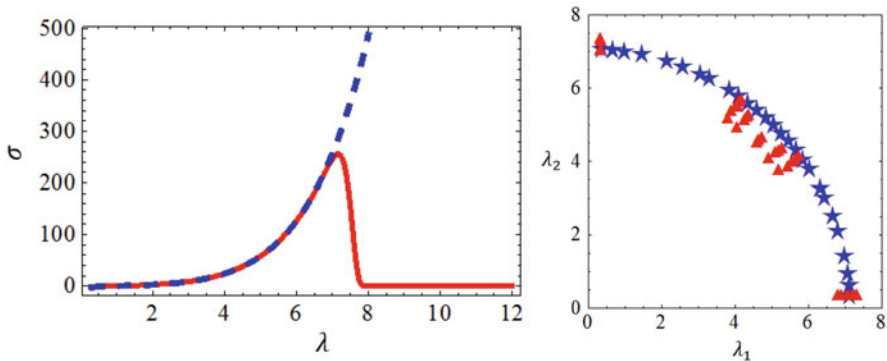


Fig. 1 Left: Cauchy stress [MPa] versus stretch: dashed line denotes the intact model; solid line denotes the model with failure. Right: Failure envelope for biaxial tension: theory (stars) versus experiment (triangles)

The stress–stretch curve for uniaxial tension is shown on the left of Fig. 1. The bounded strain energy automatically provides the bounded stress and the limit point on the diagram.

This same model was also used to create the failure envelope in biaxial tension – Fig. 1 right. The theoretical critical points were calculated from the condition of the vanishing determinant of the Hessian of strain energy [15].

In summary, we showed a simple way to account for material failure in the constitutive law without introducing internal variables. In this case, all material constants can be fitted in macroscopic experiments. Despite its simplicity, the proposed formulation allows attacking various interesting problems related with the onset of damage. Some of them are considered in the next three subsections.

2.2 Cavitation

Cavitation is the phenomenon of a sudden *irreversible* expansion of micro-voids into the visible macroscopic voids. Gent and Lindley [18] nicely demonstrated this phenomenon in tension experiments on the poker-chip rubber samples – Fig. 2 left. Such thin samples exposed to uniaxial tension in out-of-plane direction exhibit highly triaxial deformation – hydrostatic tension. The hydrostatic tension, in its turn, leads to the void expansion – cavitation.

Mathematically the void expansion can be described by the following integral formula [1]:

$$p(\lambda_a) = \int_1^{\lambda_a} \frac{1}{\lambda^3 - 1} \frac{d\psi}{d\lambda} d\lambda, \tag{9}$$

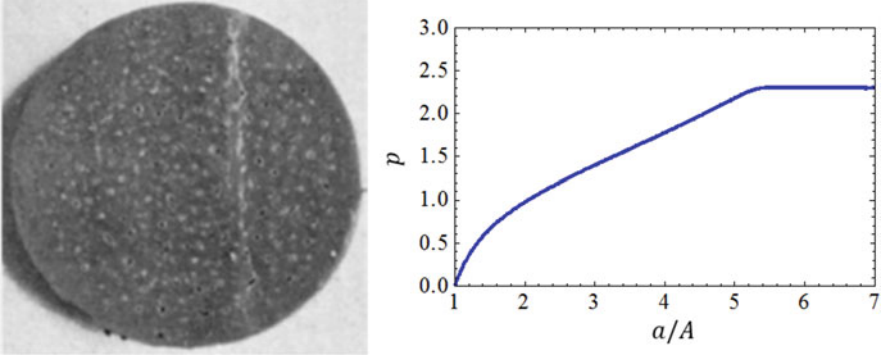


Fig. 2 Left: Grown voids in the poker-chip test [18]. Right: Hydrostatic tension [MPa] versus hoop stretch for void growth

where p is the hydrostatic tension; λ is the hoop stretch; $\lambda_a = a/A$ with A and a denoting the initial and current radius of the void accordingly; and the strain energy is expressed in terms of the principal stretches for incompressible material

$$\psi(\lambda_1, \lambda_2, \lambda_3) = \psi(\lambda^{-2}, \lambda, \lambda). \quad (10)$$

Ultimately $\lambda_a \rightarrow \infty$ and (9) should converge to the critical tension [19]

$$p_{\text{cr}} = \int_1^\infty \frac{1}{\lambda^3 - 1} \frac{d\psi}{d\lambda} d\lambda. \quad (11)$$

In the case of neo-Hookean material model we define the strain energy as follows:

$$\psi = (\mu/2)(I_1 - 3), \quad I_1 = \lambda^{-4} + 2\lambda^2, \quad (12)$$

where μ is the shear modulus.

Then, substitution of (12) in (11) yields

$$p_{\text{cr}} = (5/2)\mu. \quad (13)$$

The latter result was used by Gent and Lindley [18] to explain the cavitation phenomenon theoretically. Such explanation proliferated in the subsequent literature and it tacitly relies upon the following assumptions:

- cavitation is a purely elastic phenomenon;
- neo-Hookean material model is applicable for analysis of large stretches;
- the obtained critical hydrostatic tension (13) is universal for all materials with the given initial shear modulus μ .

All these assumptions are incorrect:

- [a] if the cavitation phenomenon was purely elastic, then we would not observe it after unloading while we do observe it;
- [b] Neo-Hookean model is only relevant for very moderate stretches not exceeding values of 1.4 while the critical hydrostatic tension is achieved for much greater stretches;
- [c] the integral in (11) converges to the finite critical tension for the neo-Hookean material model while it does not converge for more realistic material models [20].

We emphasize that the very fact of irreversibility of the void growth clearly indicates that cavitation is related to damage and only theories describing damage can be used for the explanation of the phenomenon. Particularly, the model with energy limiters presented in the previous subsection can be used in (9). The tension–stretch curve for this model is presented in Fig. 2 right [21]. The horizontal line gives the critical tension of ~ 2.3 MPa that can be calculated from (11). The experimental estimate of the critical tension of about ~ 2.7 MPa [18] is encouraging for the theoretical analysis. Various models without failure can be enhanced with energy limiters to provide convergence to critical tensions [20, 22]. Without the limiters such models would not be able to explain the cavitation phenomenon.

The role of inertia forces and viscosity in cavitation was uncovered in [23] while the thermal effects were considered in [24] for the first time.

We note, in passing, that the specific constitutive model for natural rubber described in the previous subsection nicely fits experimental data in uniaxial, biaxial, and triaxial (cavitation) states of deformation including failure.

2.3 Strength of Soft Composites

Soft composites comprise soft matrix and reinforcements of various shapes. They are used in various applications ranging from rubber bearings to soft robots and advanced biomedical devices. Soft biocomposites can be created, for example, by the natural process of tissue calcification, etc. The reinforcement stiffens a soft ground matrix. What is the effect of reinforcement on the strength of the composite? The answer is not evident at all.

We developed micromechanical approach to analysis of the onset of failure in soft composites combining the elasticity with energy limiters and high fidelity generalized method of cells (HFGMC) [25].

We used the approach to study strength of an idealized calcified aneurysmal tissue [26]. Particularly, we analyzed the effect of the varying amount of calcification (10%, 40%, and 70%), i.e. the relative volume of the hard inclusion within the periodic elementary cell, on the tissue stiffness and strength. We found that the increase of the relative volume of calcium particles unconditionally led to the stiffening of the tissue. At the same time, the strength did not increase in the most considered cases – it could significantly decrease. Quantitatively, the strength

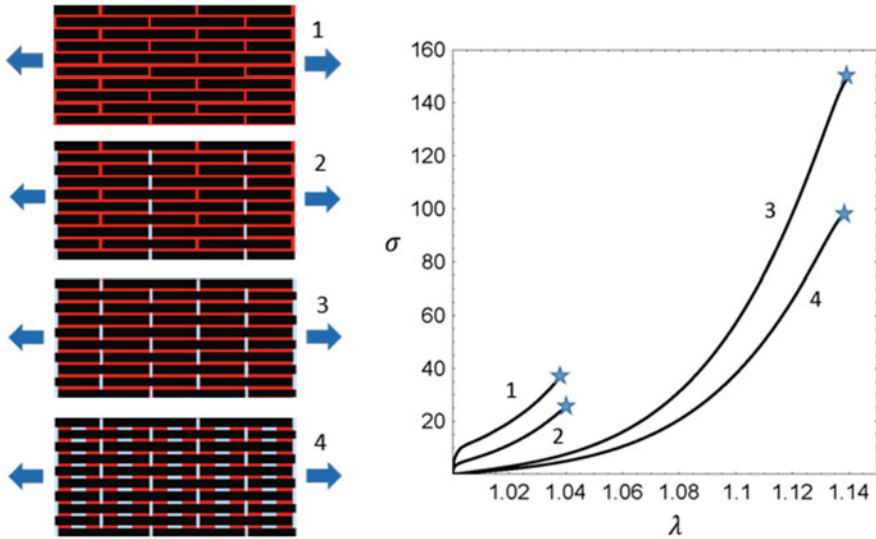


Fig. 3 Staggered soft composites comprising matrix (red) and reinforcing platelets (black) and pre-existing cracks (white) under uniaxial tension are shown on the left. Corresponding Cauchy stress – stretch curves in uniaxial tension are shown on the right. Stars designate critical points beyond which static solution does not exist – strength [27]

decrease could vary from 10% to 40% and more. One might find it contrary to intuition that the strength can decrease while the stiffness always increases with calcification. This interesting finding emphasizes the difference between the concepts of stiffness and strength which is not always appreciated. The strength of a composite is significantly affected by the locally nonuniform state of deformation. Small hard particles rather than big ones can be stress concentrators amplifying the likelihood of the local material failure. Also the hard particles restrain deformation in their vicinity creating the state of hydrostatic tension which, in its turn, may trigger cavitation with the subsequent fracturing. The obtained results have limitations because an ideally periodic distribution of calcified particles was assumed in computations while in reality the distribution is random. Thus, additional research in stochastic mechanics of failure analysis is required.

The approach developed in [25] was also used in [27] to simulate strength of bioinspired soft composites with the staggered alignment of hard platelets in a soft matrix. The strength was analyzed for different cases of the composite material with various amounts of hard inclusions and various pre-existing cracks – Fig. 3.

We found, for example, that the soft matrix material placed between short edges of platelets with high aspect ratio was the weakest link of the composite. In these areas the strength was reached. Amazingly, by deleting soft material or introducing pre-existing cracks in these dangerous areas it was possible to significantly increase (~ 4 times) the strength of the composite. Such finding might seem contrary to intuition at first glance. However, the pre-existing cracks actually relieved the stress

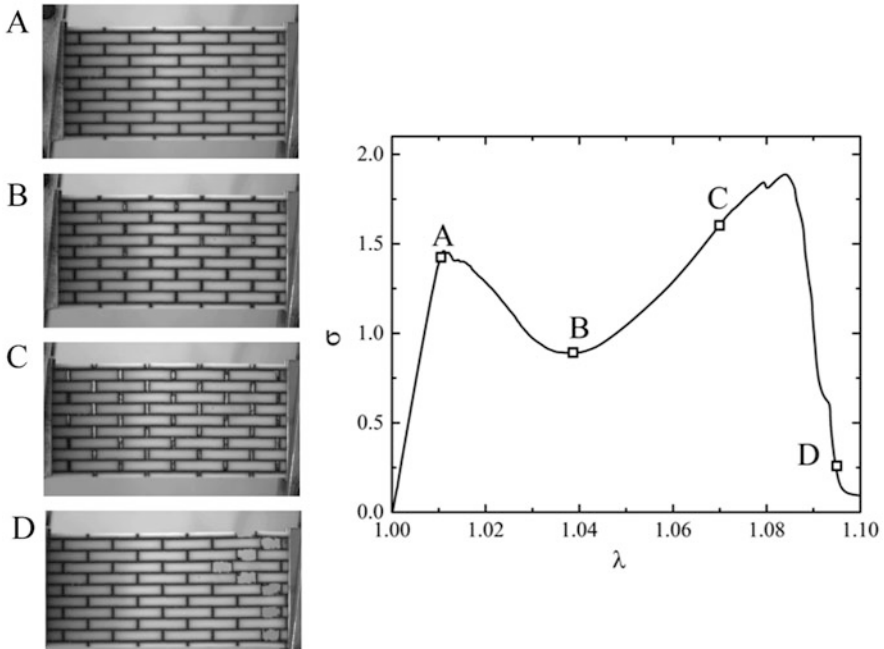


Fig. 4 Experiments with 3D printed soft composite: snapshots on the left correspond to the points on the stress – stretch curve on the right [27]

and strain concentrators providing greater material resistance. The main load bearing area of the matrix became the region connecting long edges of platelets. This region was predominantly in the state of shear. The failure of the soft matrix in shear was responsible for the overall strength of the composite. Importantly, the overall strength did not exceed the strength of the matrix material in the uniaxial tension.

In order to validate the computational analysis described above, we performed experiments on 3D printed composites – Fig. 4.

Unfortunately, the 3D printing procedure did not allow to create the natural rubber material used in simulations. Instead, soft interfaces were printed in soft hyperelastic digital material and stiff platelets were printed in rigid VeroWhite polymer. Samples were fabricated by using a multi-material Polyjet technique with a help of the 3D-printer Objet Connex 260. Performing the uniaxial tension test shown in Fig. 4, we observed that after reaching the critical level of loading – point A, the soft matrix at the short platelet edges ruptured. This led to a significant drop in stress level during the following loading up to point B. Then the shear deformation in the soft matrix along the lengthy edges of platelets dominated until approximately point C soon after which the ultimate stress – strength – was reached and material started disintegrating as at point D. This observation qualitatively supported the numerically predicted phenomena – Fig. 3 – showing that the catastrophic failure originated in the soft interface phase, and it had a significant

influence on the overall strength of the composite. We emphasize the qualitative rather than quantitative resemblance in view of the different matrix materials used in simulations and experiments. The resemblance is encouraging.

2.4 Prediction of Crack Direction

In this subsection, we show how to predict the onset of cracks including their direction by using the elasticity with energy limiters and strong ellipticity condition.

We start with a brief description of the underlying theory [28]. Designating increments with tildes it is possible to derive incremental equations of momenta balance and constitutive law

$$\rho_0 \ddot{\tilde{\mathbf{y}}} = \text{Div} \tilde{\mathbf{P}}, \quad \tilde{\mathbf{P}} \mathbf{F}^T + \mathbf{P} \tilde{\mathbf{F}}^T = (\tilde{\mathbf{P}} \mathbf{F}^T + \mathbf{P} \tilde{\mathbf{F}}^T)^T, \quad \tilde{\mathbf{P}} = \partial^2 \psi / \partial \mathbf{F} \partial \mathbf{F} : \tilde{\mathbf{F}}. \quad (14)$$

Alternatively, these incremental equations can be reformulated in the Eulerian form where the current configuration Ω is referential

$$\rho \ddot{\tilde{\mathbf{y}}} = \text{div} \tilde{\boldsymbol{\sigma}}, \quad \tilde{\boldsymbol{\sigma}} + \boldsymbol{\sigma} \tilde{\mathbf{L}}^T = (\tilde{\boldsymbol{\sigma}} + \boldsymbol{\sigma} \tilde{\mathbf{L}}^T)^T, \quad \tilde{\boldsymbol{\sigma}} = \mathbb{A} : \tilde{\mathbf{L}}, \quad (15)$$

where $\rho = J^{-1} \rho_0$; $\boldsymbol{\sigma} = J^{-1} \mathbf{P} \mathbf{F}^T$ is the Cauchy stress tensor and $(\text{div} \tilde{\boldsymbol{\sigma}})_i = \partial \tilde{\sigma}_{ij} / \partial y_j$; $\tilde{\boldsymbol{\sigma}} = J^{-1} \tilde{\mathbf{P}} \mathbf{F}^T$ is the incremental Cauchy stress; $\tilde{\mathbf{L}} = \tilde{\mathbf{F}} \mathbf{F}^{-1}$ is the incremental velocity gradient; \mathbb{A} is the fourth order elasticity tensor with Cartesian components

$$A_{ijkl} = J^{-1} F_{js} F_{lr} \frac{\partial^2 \psi}{\partial F_{is} \partial F_{kr}}. \quad (16)$$

For the strain energy defined by (5), we further calculate

$$\frac{\partial \psi}{\partial F_{is}} = \frac{\partial \psi}{\partial W} \frac{\partial W}{\partial F_{is}} = \exp[-W^m \Phi^{-m}] \frac{\partial W}{\partial F_{is}}, \quad (17)$$

and

$$\frac{\partial^2 \psi}{\partial F_{is} \partial F_{kr}} = \left(\frac{\partial^2 W}{\partial F_{is} \partial F_{kr}} - m W^{m-1} \Phi^{-m} \frac{\partial W}{\partial F_{kr}} \frac{\partial W}{\partial F_{is}} \right) \exp[-W^m \Phi^{-m}]. \quad (18)$$

Substitution of (18) in (16) yields

$$A_{ijkl} = J^{-1} F_{js} F_{lr} \left(\frac{\partial^2 W}{\partial F_{is} \partial F_{kr}} - m W^{m-1} \Phi^{-m} \frac{\partial W}{\partial F_{kr}} \frac{\partial W}{\partial F_{is}} \right) \exp[-W^m \Phi^{-m}]. \quad (19)$$

We look for a plane wave solution of the incremental initial boundary value problem

$$\tilde{\mathbf{y}} = \mathbf{r}g(\mathbf{s} \cdot \mathbf{y} - vt), \quad (20)$$

where \mathbf{r} and \mathbf{s} are the unit vectors in the directions of wave polarization and wave propagation, respectively; and v is the wave speed.

Substituting for $\tilde{\mathbf{L}} = \text{grad} \tilde{\mathbf{y}} = \partial \tilde{\mathbf{y}} / \partial \mathbf{y}$ from (20) to (15)₃, we get the incremental stress $\tilde{\boldsymbol{\sigma}}$. Then, substituting for $\tilde{\mathbf{y}}$ from (20) and $\tilde{\boldsymbol{\sigma}}$ to the linear momentum balance (15)₁, we get

$$\rho v^2 \mathbf{r} = \boldsymbol{\Lambda}(\mathbf{s}) \mathbf{r}, \quad (21)$$

where $\boldsymbol{\Lambda}(\mathbf{s})$ is the acoustic tensor with Cartesian components

$$\Lambda_{ik} = A_{ijkl} s_j s_l. \quad (22)$$

Taking scalar product of (21) with \mathbf{r} , we obtain for the wave speed

$$J \rho v^2 = \mathbf{J} \mathbf{r} \cdot \boldsymbol{\Lambda} \mathbf{r} = f_1 f_2, \quad (23)$$

where

$$\begin{aligned} f_1 &= f_3 - m W^{m-1} \Phi^{-m} f_4^2, \\ f_2 &= \exp[-W^m \Phi^{-m}], \\ f_3 &= s_j s_l r_i r_k F_{js} F_{lr} \partial^2 W / \partial F_{is} \partial F_{kr}, \\ f_4 &= r_k s_l F_{lr} \partial W / \partial F_{kr}. \end{aligned} \quad (24)$$

The positive wave speed corresponds to the mathematical condition of the strong ellipticity of the incremental initial boundary value problem. Zero wave speed mathematically means violation of the strong ellipticity condition and, physically, it means inability of the material to propagate a wave in direction \mathbf{s} . The latter notion can also be interpreted as the onset of a crack perpendicular to \mathbf{s} .

Consider, for example, longitudinal wave (P-wave) and transverse wave (S-wave) in plane of a material sheet. Denoting the unit vectors in the plane by \mathbf{e}_1 and \mathbf{e}_2 , we can write



Fig. 5 Great East Japan Earthquake in 2011: bridge rubber bearings on the left and the horizontal crack is observed on the right [33]

$$\mathbf{s} = \mathbf{r} = \cos \alpha \mathbf{e}_1 + \sin \alpha \mathbf{e}_2 \quad (25)$$

for the P-wave and

$$\begin{aligned} \mathbf{s} &= \cos \alpha \mathbf{e}_1 + \sin \alpha \mathbf{e}_2, \\ \mathbf{r} &= -\sin \alpha \mathbf{e}_1 + \cos \alpha \mathbf{e}_2 \end{aligned} \quad (26)$$

for the S-wave, where α is unknown angle in plane.

Then, we have from (23) for the vanishing wave speed

$$J\rho v^2(\mathbf{F}, \alpha) = f_1(\mathbf{F}, \alpha) f_2(\mathbf{F}) = 0. \quad (27)$$

This condition can be explained mathematically as follows. The Rayleigh quotient rule for the given \mathbf{s} states that $\mathbf{z} \cdot \Lambda(\mathbf{s})\mathbf{z}/(\mathbf{z} \cdot \mathbf{z})$ is minimized by the first eigenvector $\mathbf{z} = \mathbf{r}$ and $\zeta = \mathbf{r} \cdot \Lambda(\mathbf{s})\mathbf{r}/(\mathbf{r} \cdot \mathbf{r})$ is its minimum value, which is the smallest eigenvalue of $\Lambda(\mathbf{s})$. Obviously, this eigenvector \mathbf{r} might not obey conditions of the longitudinal ($\mathbf{r} = \mathbf{s}$) or transverse ($\mathbf{r} \cdot \mathbf{s} = 0$) waves. However, the situation changes when we assume the minimum value in advance: $\zeta = \mathbf{r} \cdot \Lambda(\mathbf{s})\mathbf{r} = 0$. In this particular case both longitudinal and transverse waves can be found by the direct solution of $\mathbf{r} \cdot \Lambda(\mathbf{s})\mathbf{r} = 0$. Any \mathbf{r} providing the zero minimum eigenvalue becomes the corresponding eigenvector. The very existence of the longitudinal ($\mathbf{r} = \mathbf{s}$) or transverse ($\mathbf{r} \cdot \mathbf{s} = 0$) waves comes directly from the computation itself.

The described approach was used to predict the onset of cracks and their direction in a series of publications [29–32].

Bridge rubber bearings undergo a simultaneous compression and shear under earthquakes and cracks appear in them in the direction of shear – Fig. 5. Such shear cracks were predicted by the analysis described above [29].

This analysis included the assumption of material incompressibility. However, the incompressibility constraint suppresses longitudinal waves and, thus, valuable information about cracks can be missed. The latter issue was explored in [30] where the incompressibility constraint was abandoned. It was found, indeed, that the

constraint could turn into a Trojan Horse in the analytical calculations and an important information about cracks could be missed. Particularly, in the cases of uniaxial tension and pure shear, it was found that namely longitudinal waves helped to predict cracks perpendicular to the direction of tension. Amazingly, it was also found that the transverse wave led to the prediction of cracks whose direction was close to the direction of tension. The latter prediction seemed unrealistic; however, such cracks in the direction of tension were found in recent experiments [34]!

The onset of cracks in anisotropic soft materials – arterial wall – was considered in [31, 32]. Particularly in [32], we developed two constitutive models with 16 and 8 structure tensors to account for anisotropy and failure of the wall. The intact material behavior was calibrated based on the experimental data for human adventitia and energy limiters were introduced to describe failure. These models were used in analysis of the loss of strong ellipticity in uniaxial tension and pure shear in circumferential and axial directions of the artery and in biaxial tension. Directions of possible cracks were obtained from the condition of the vanishing speed of the superimposed longitudinal and transverse waves. The vanishing longitudinal wave speed predicted the appearance of cracks in the direction perpendicular to tension in uniaxial tension and pure shear. As in the case of isotropic material discussed above, such prediction would be suppressed by the incompressibility constraint. The vanishing transverse wave speed predicted the appearance of cracks in the direction inclined to tension in uniaxial tension and pure shear. Equibiaxial stretching can lead to the appearance of cracks in any direction despite the anisotropy of material. The inclined cracks oriented along the bundles of collagen fibers have been found in experiments [35].

3 Fracture as Damage Localization

Fracture in the form of cracks was first considered by Griffith [36]. Analogously to the strength-of-materials approach, he suggested a criterion of growth of pre-existing cracks based on the global energy balance. Such integral balance ignores the role of the strain and stress concentrations at the tip of the crack and, therefore, it is open to criticism [37]. There are various conceptual approaches to fracture in the literature. We believe that fracture should be incorporated in the constitutive description of materials and crack initiation and propagation should be an outcome of the solution of the clearly formulated initial boundary value problems. In this spirit, there are two main approaches to modeling fracture – surface and bulk crack models.

Surface crack models, or cohesive surface models (CSM), consider continuum enriched with discontinuities along surfaces with additional traction-displacement-separation constitutive laws [37–47]. If the location of the separation surface is known in advance (e.g. fracture along weak interfaces), then the use of CSM is natural. Otherwise, the insertion of cracks in the bulk in the form of separation surfaces remains an open problem, which includes definition of criteria for crack nucleation, orientation, branching, and arrest. Besides, the CSM approach presumes

the simultaneous use of two different constitutive models: one for the cohesive surface and another for the bulk, for the same real material. Certainly, a correspondence between these two constitutive theories is desirable yet not promptly accessible.

Bulk crack models, or continuum damage mechanics (CDM), introduce failure in constitutive laws in the form of the falling stress–strain curves [48–55].¹ Damage nucleation, propagation, branching, and arrest naturally come out of the constitutive laws. Unfortunately, numerical simulations based on bulk failure laws show the so-called pathological mesh sensitivity, which means that finer meshes lead to narrower damage localization areas. In the limit case, the energy dissipation in damage tends to zero with the diminishing size of the computational mesh. This physically unacceptable mesh sensitivity is caused by the lack of a characteristic length in the traditional formulation of continuum mechanics. To surmount the latter pitfall gradient- or integral-type nonlocal continuum formulations are used where a characteristic length is incorporated to limit the size of the spatial damage localization [56–60]. In the gradient-type approaches, for example, an additional internal damage variable is introduced together with additional differential equation of reaction-diffusion type. This equation has a small parameter – the characteristic length – as a scaling factor for the highest spatial derivatives of the damage variable. The characteristic length provides solution of the boundary layer type. This layer is interpreted as a diffused crack of finite thickness rather than a surface of discontinuity.

A special choice of the additional regularizing equation, called phase-field approach, gained popularity in recent years [61–63]. It is claimed that the phase-field formulation provides convergence of the diffused crack to the surface of discontinuity under the decrease of the characteristic length. Thus, the characteristic length is interpreted as a purely numerical parameter which can be varied. However, the case of the uniform uniaxial tension shows that, in the phase-field formulation, the characteristic length is a physical parameter linked to material strength² and it cannot be varied. Thus, the phase-field approach is a possible yet not superior regularization of the gradient type.

The regularization strategy rooted in the nonlocal continua formulations is attractive because it is lucid mathematically. Unluckily, the generalized nonlocal continua theories are based (often tacitly) on the physical assumption of long-range particle interactions while the actual particle interactions are short-range – on nanometer or angstrom scale. Therefore, the physical basis for the nonlocal models appears disputable. A more physically based treatment of the pathological mesh sensitivity of the bulk failure simulations should likely include multi-physics coupling. Such a

¹These works were not devoted to soft materials per se.

²For example, the authors of [63] rightfully note that “although the length-scale parameter associated with the phase-field approximation is introduced as a numerical parameter it is, in fact, a material parameter that influences the critical stress at which crack nucleation occurs.”



Fig. 6 Left: idealized crack with zero thickness; middle: visible closed crack in unloaded tire; right: realistic bulk crack with finite thickness l

theory coupling mass flow (sink) and finite elastic deformation is considered in the next subsections.

3.1 Material Sink Formulation

We can see crack surfaces and we rightfully conclude that these surfaces are a result of material separation. However, people usually and tacitly make one more logical step and assume that the separation is a result of debonding of two adjacent atomic or molecular layers – Fig. 6 left. At the first thought, the latter assumption is the simplest one and it appeals to intuition. At the second thought, it is possible to realize that the assumption is wrong because cracks are visible by a naked eye – Fig. 6 middle. Indeed, if the separation was between two adjacent atomic layers, then we would not see closed cracks because our eye can only distinguish objects on the scale of microns and not angstroms. Thus, the crack surfaces are not created by two adjacent atomic layers – they are created by a massive bond breakage spread over a region with characteristic length l – Fig. 6 right.

It is crucial to realize that the process of the bond breakage is diffusive rather than confined to one atomic plane. Some atoms fly out of the bulk material. Generally, we cannot see them because of their very small amount (as compared to the bulk). Sometimes, we can see them – remember the dust which comes out of cracks in brittle concrete. The characteristic length of the damage region is so big in the latter case that we can see small pieces of concrete that left the bulk during fracture.

Summarizing the qualitative picture of the crack formation we note that material sinks within the characteristic small region of damage. Such notion gives rise to the mathematical formulation in which momenta and mass balance are coupled [64].

Thus, the mass balance equations should be coupled with $(1)_{1,2}$ in Ω_0

$$\text{Div} \mathbf{s}_0 + \xi_0 = 0, \tag{28}$$

where \mathbf{s}_0 and ξ_0 are the referential mass flux and source (sink) accordingly.

The corresponding natural boundary condition expresses this same mass balance law on the boundary $\partial\Omega_0$

$$\mathbf{s}_0 \cdot \mathbf{n}_0 = 0. \quad (29)$$

We note that we use the mass balance in the reduced form: $\text{Divs}_0 + \xi_0 = 0$; instead of the general form: $\dot{\rho}_0 = \text{Divs}_0 + \xi_0$; because we are only interested in pre- and post-cracked states while the transition – bond rupture – process is so fast that it can be ignored. Such simplification is analogous to consideration of the buckling process in thin-walled structures. In the latter case, pre- and post-buckled states of a structure are usually analyzed by using a time-independent approach while the very process of the fast dynamic transition to the buckled state is ignored in analysis by dropping the inertia terms from the momentum balance equation.

We define constitutive equations for the stress [64]

$$\mathbf{P} = (\rho_0/\bar{\rho}_0) \partial W / \partial \mathbf{F}, \quad (30)$$

mass sink

$$\xi_0 = \beta \bar{\rho}_0 H(\gamma) \exp[-W^m \Phi^{-m}] - \beta \rho_0, \quad (31)$$

and mass flux

$$\mathbf{s}_0 = \kappa H(\gamma) \exp[-W^m \Phi^{-m}] J(\mathbf{F}^T \mathbf{F})^{-1} \text{Grad} \rho_0, \quad (32)$$

where $\bar{\rho}_0 = \rho_0(t=0)$ is the initial referential density; $\beta > 0$ and $\kappa > 0$ are material constants; $H(\gamma)$ is a unit step function, i.e. $H(\gamma) = 0$ if $\gamma < 0$ and $H(\gamma) = 1$ otherwise; the switch parameter $\gamma \in (-\infty, 0]$ is necessary to prevent from material healing and it is defined by the evolution equation $\dot{\gamma} = -H(\varepsilon - \rho_0/\bar{\rho}_0)$, $\gamma(t=0) = 0$ where $0 < \varepsilon \ll 1$ is a dimensionless precision constant.

It is important to emphasize that the formulation presented in this subsection is a generalization of elasticity with energy limiters described above. Indeed, the elasticity with energy limiters emerges as a particular case where there is no damage localization via diffusion of broken bonds. In the latter case, we have the vanishing mass flux: $\mathbf{s}_0 = \mathbf{0}$; and sink: $\xi_0 = 0$. In view of the zero material sink we calculate from (31): $\rho_0/\bar{\rho}_0 = H(\gamma) \exp[-W^m \Phi^{-m}]$. Since the irreversibility of the process is not important in this case and $H(\gamma) \equiv 1$, we further simplify: $\rho_0/\bar{\rho}_0 = \exp[-W^m \Phi^{-m}]$. Substitution of the latter formula in (30) yields: $\mathbf{P} = \exp[-W^m \Phi^{-m}] \partial W / \partial \mathbf{F}$, which coincides with (7).

3.2 Dynamic Crack Propagation

Most works on modeling cracks consider quasi-static crack propagation. Yet in reality, most cracks propagate dynamically unless they are highly restrained. Indeed, the onset and localization of damage are usually related to the loss of the static

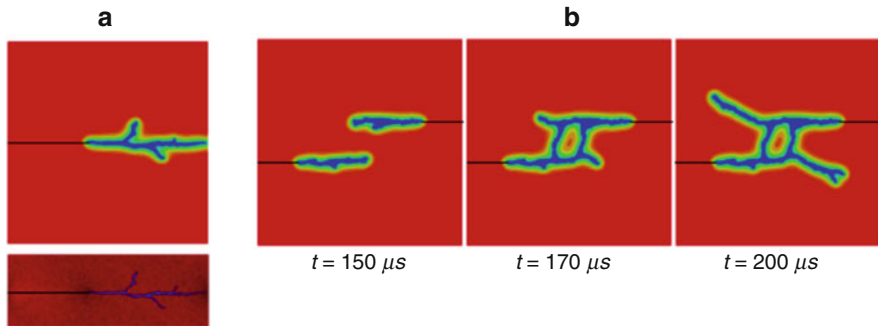


Fig. 7 (a) Propagation of Mode I crack in aneurysm material in current (top) and referential (bottom) configurations; (b) crack bridging and kinking

stability of a structure. The process of crack propagation becomes dynamic. The latter notion is not properly appreciated in the literature and many authors prefer static analysis over the dynamic one because of its relative simplicity rather than physical adequacy. A review of the crack propagation in rubberlike materials can be found in [65].

We implemented the material sink formulation presented above in analysis of dynamic crack propagation in aneurysm material and we refer to [66] for details. Nevertheless, we note that substitution of constitutive equations (31) and (32) in the mass balance law (28) yields the following second order partial differential equation with respect to the referential mass density, ρ_0 ,

$$l^2 \text{Div}\{H(\gamma) \exp[-W^m \Phi^{-m}] J(\mathbf{F}^T \mathbf{F})^{-1} \text{Grad} \rho_0\} + \bar{\rho}_0 H(\gamma) \exp[-W^m \Phi^{-m}] - \rho_0 = 0. \quad (33)$$

Remarkably, we do not need to know material constants κ and β separately anymore. We only need to know their ratio, which gives us the characteristic length

$$l = \sqrt{\kappa/\beta}. \quad (34)$$

Such length serves as a small multiplier for the highest (second) spatial derivative of the mass density and, consequently, it causes solution of the boundary layer type. This boundary layer regularizes the crack width suppressing the pathological mesh sensitivity.

Some results of modeling propagation of a single crack and bridging of two cracks are shown in Fig. 7. These simulations led to the following interesting conclusions.

First, the inertia forces play crucial role at the tip of the propagating crack. If inertia is not canceled together with the material stiffness, then cracks tend to nonphysically widen with the increasing speed of their propagation. Most existing

models of cracks completely ignore this fact and they do not cancel inertia when they cancel stiffness. Remarkably, the very recent works based on the phase-field formulations [67, 68] started recognizing the importance of canceling inertia. Needless to say, the simultaneous cancellation of stiffness and inertia are a direct consequence of the material sink formulation presented in this chapter.

Second, the proposed material sink formulation allows suppressing the *strong* or the classical pathological mesh-dependence linked to the zero energy fracture. The latter is due to the fact that the augmented initial boundary volume problem enforces characteristic length and solutions of the boundary layer type. The boundary layer, associated with the crack thickness does not vanish under the mesh refinement.

Third, we observed a *weak* mesh-dependence, which we defined as the effect of the mesh shape and size on the specific crack pattern. We observed that various meshes caused slightly different crack patterns for the same amount of dissipated energy. The weak mesh-dependence remained even after a significant mesh refinement, which showed that the regularized formulations were not a universal solution for any mesh sensitivity as many would expect. The weak mesh-dependence is similar to the effect of structural inhomogeneities in real materials, which affect the crack path depending on the specific sample under consideration. Though all samples are made of the same material they have various microstructural patterns and, consequently, slightly different propagating cracks.

4 Final Remarks

We presented review of our recent developments concerning analysis of failure and fracture in soft materials. Approaches for modeling failure and fracture are different. Failure is identified with the onset of material instability and damage. We considered such instability as a direct consequence of the bounded strain energy density. The bounded strain energy, in its turn, follows from the fact that the number of physical particles and their integral bond energy are limited. We presented a general formula allowing for the enforcement of energy bounds in the known hyperelastic models of soft materials and we called it elasticity with energy limiters.

After the onset, material damage localizes into cracks and they propagate. We call this process fracture. To model fracture, we introduced an augmented formulation, in which momenta and mass balance are coupled. The mass balance equation reflects upon the physical fact that broken bonds are diffused in the area of characteristic size rather than confined to a single atomic plane. The mass balance equation regularizes numerical simulations creating solutions of the boundary layer type and suppressing the pathological mesh-dependence. The latter means that refining the mesh one would not be able to reduce fracture energy to zero.

It is remarkable that the approaches described in the present work are based on two physical observations only: bond energy is bounded and broken bonds are diffused. Based on these observations it was possible to formulate theories of failure and fracture without introducing any internal variables.

Acknowledgment This research was supported by the Israel Science Foundation (grant No. 394/20).

References

1. Volokh KY (2019) *Mechanics of soft materials*. Springer, Singapore
2. Truesdell C, Noll W (2004) *The non-linear field theories of mechanics*. Springer, Berlin
3. Simo JC (1987) On a fully three-dimensional finite strain viscoelastic damage model: formulation and computational aspects. *Comp Meth Appl Mech Eng* 60:153–173
4. Govindjee S, Simo JC (1991) A micro-mechanically based continuum damage model of carbon black-filled rubbers incorporating the Mullins effect. *J Mech Phys Solids* 39:87–112
5. Johnson MA, Beatty MF (1993) A constitutive equation for the Mullins effect in stress controlled in uniaxial extension experiments. *Cont Mech Therm* 5:301–318
6. Miehe C (1995) Discontinuous and continuous damage evolution in Ogden-type large-strain elastic materials. *Eur J Mech A/Solids* 14:697–720
7. De Souza Neto EA, Peric D, Owen DRJ (1998) Continuum modeling and numerical simulation of material damage at finite strains. *Arch Comp Meth Eng* 5:311–384
8. Ogden RW, Roxburgh DG (1999) A pseudo-elastic model for the Mullins effect in filled rubber. *Proc Roy Soc Lond Ser A* 455:2861–2877
9. Menzel A, Steinmann P (2001) A theoretical and computational framework for anisotropic continuum damage mechanics at large strains. *Int J Solids Struct* 38:9505–9523
10. Guo Z, Sluys L (2006) Computational modeling of the stress-softening phenomenon of rubber like materials under cyclic loading. *Eur J Mech A/Solids* 25:877–896
11. De Tommasi D, Puglisi G, Saccomandi G (2008) Localized vs diffuse damage in amorphous materials. *Phys Rev Lett* 100:085502.
12. Dal H, Kaliske M (2009) A micro-continuum-mechanical material model for failure of rubber-like materials: application to ageing-induced fracturing. *J Mech Phys Solids* 57:1340–1356
13. Volokh KY (2013) Review of the energy limiters approach to modeling failure of rubber. *Rubber Chem Technol* 86:470–487
14. Volokh KY (2007) Hyperelasticity with softening for modeling materials failure. *J Mech Phys Solids* 55:2237–2264
15. Volokh KY (2010) On modeling failure of rubberlike materials. *Mech Res Commun* 37:684–689
16. Volokh KY (2014) On irreversibility and dissipation in hyperelasticity with softening. *J Appl Mech* 81:074501
17. Hamdi A, Nait Abdelaziz M, Ait Hocine N, Heuillet P, Benseddiq N (2006) A fracture criterion of rubber-like materials under plane stress conditions. *Polym Test* 25:994–1005
18. Gent AN, Lindley PB (1959) Internal rupture of bonded rubber cylinders in tension. *Proc Roy Soc A* 2:195–205
19. Ball JM (1982) Discontinuous equilibrium solutions and cavitation in nonlinear elasticity. *Phil Trans Roy Soc Lond A* 306:557–610
20. Lev Y, Volokh KY (2016) On cavitation in rubberlike materials. *J Appl Mech* 83:044501
21. Volokh KY (2011) Cavitation instability in rubber. *Int J Appl Mech* 3:29311
22. Volokh KY (2015) Cavitation instability as a trigger of aneurysm rupture. *Biomech Model Mechanobiol* 14:1071–1079
23. Faye A, Rodriguez-Martnez JA, Volokh KY (2017) Spherical void expansion in rubber-like materials: the stabilizing effects of viscosity and inertia. *Int J Non-Linear Mech* 92:118–126
24. Lev Y, Faye A, Volokh KY (2019) Thermoelastic deformation and failure of rubberlike materials. *J Mech Phys Solids* 122:538–554

25. Aboudi J, Volokh KY (2015) Failure prediction of unidirectional composites undergoing large deformations. *J Appl Mech* 82:071004
26. Volokh KY, Aboudi J (2016) Aneurysm strength can decrease under calcification. *J Mech Behav Biomed Mater* 57:164–174
27. Slesarenko V, Volokh KY, Aboudi J, Rudykh S (2017) Understanding the strength of bioinspired soft composites. *Int J Mech Sci* 131–132:171–178
28. Volokh KY (2017) Loss of ellipticity in elasticity with energy limiters. *Eur J Mech A Solids* 63:36–42
29. Mythravaruni P, Volokh KY (2018) Failure of rubber bearings under combined shear and compression. *J Appl Mech* 85:074503
30. Mythravaruni P, Volokh KY (2019) On incompressibility constraint and crack direction in soft solids. *J Appl Mech* 86:101004
31. Volokh KY (2019) Constitutive model of human artery adventitia enhanced with a failure description. *Mech Soft Mater* 1:8
32. Mythravaruni P, Volokh KY (2020) On the onset of cracks in arteries. *Mol Cell Biomech* 17:1–17
33. Takahashi Y (2012) Damage of rubber bearings and dumpers of bridges in 2011 great East Japan earthquake. Proceedings of the International Symposium on Engineering, Lessons Learned from the 2011 Great East Japan Earthquake, March 1–4, Tokyo, Japan
34. Lee S, Pharr M (2019) Sideways and stable crack propagation in a silicone elastomer. *PNAS* 116:9251–9256
35. Sugita S, Matsumoto T (2017) Local distribution of collagen fibers determines crack initiation site and its propagation direction during aortic rupture. *Biomech Model Mechnobiol* 17:577–587
36. Griffith AA (1921) The phenomena of rupture and flow in solids. *Philos Trans R Soc Lond A* 221:163–198
37. Volokh KY, Trapper P (2008) Fracture toughness from the standpoint of softening hyperelasticity. *J Mech Phys Solids* 56:2459–2472
38. Barenblatt GI (1959) The formation of equilibrium cracks during brittle fracture. General ideas and hypotheses. Axially-symmetric cracks. *J Appl Math Mech* 23:622–636
39. Needleman A (1987) A continuum model for void nucleation by inclusion debonding. *J Appl Mech* 54:525–531
40. Rice JR, Wang JS (1989) Embrittlement of interfaces by solute segregation. *Mater Sci Eng A* 107:23–40
41. Tvergaard V, Hutchinson JW (1992) The relation between crack growth resistance and fracture process parameters in elastic-plastic solids. *J Mech Phys Solids* 40:1377–1397
42. Camacho GT, Ortiz M (1996) Computational modeling of impact damage in brittle materials. *Int J Solids Struct* 33:2899–2938
43. de Borst R (2001) Some recent issues in computational failure mechanics. *Int J Numer Meth Eng* 52:63–95
44. Xu XP, Needleman A (1994) Numerical simulations of fast crack growth in brittle solids. *J Mech Phys Solids* 42:1397–1434
45. Moes N, Dolbow J, Belytschko T (1999) A finite element method for crack without remeshing. *Int J Num Meth Eng* 46:131–150
46. Park K, Paulino GH, Roesler JR (2009) A unified potential-based cohesive model of mixed-mode fracture. *J Mech Phys Solids* 57:891–908
47. Gong B, Paggi M, Carpinteri A (2012) A cohesive crack model coupled with damage for interface fatigue problems. *Int J Fract* 137:91–104
48. Kachanov LM (1958) Time of the rupture process under creep conditions. *Izvestiia Akademii Nauk SSSR, Otdelenie Teckhnicheskikh Nauk* 8:26–31
49. Gurson AL (1977) Continuum theory of ductile rupture by void nucleation and growth: part I—yield criteria and flow rules for porous ductile media. *J Eng Mat Tech* 99:2–151

50. Voyiadjis GZ, Kattan PI (1992) A plasticity-damage theory for large deformation of solids—I. Theoretical formulation. *Int J Eng Sci* 30:1089–1108
51. Gao H, Klein P (1998) Numerical simulation of crack growth in an isotropic solid with randomized internal cohesive bonds. *J Mech Phys Solids* 46:187–218
52. Klein P, Gao H (1998) Crack nucleation and growth as strain localization in a virtual-bond continuum. *Eng Fract Mech* 61:21–48
53. Lemaitre J, Desmorat R (2005) *Engineering damage mechanics: ductile, creep, fatigue and brittle failures*. Springer, Berlin
54. Volokh KY (2004) Nonlinear elasticity for modeling fracture of isotropic brittle solids. *J Appl Mech* 71:141–143
55. Benzerga AA, Leblond JB, Needleman A, Tvergaard V (2016) Ductile failure modeling. *Int J Fract* 201:29–80
56. Pijaudier-Cabot G, Bazant ZP (1987) Nonlocal damage theory. *J Eng Mech* 113:1512–1533
57. Lasry D, Belytschko T (1988) Localization limiters in transient problems. *Int J Solids Struct* 24:581–597
58. Peerlings RHJ, de Borst R, Brekelmans WAM, de Vree JHP (1996) Gradient enhanced damage for quasi-brittle materials. *Int J Num Meth Eng* 39:3391–3403
59. de Borst R, van der Giessen E (1998) *Material instabilities in solids*. Wiley, Chichester
60. Silling SA (2000) Reformulation of elasticity theory for discontinuities and long-range forces. *J Mech Phys Solids* 48:175–209
61. Francfort GA, Marigo JJ (1998) Revisiting brittle fracture as an energy minimization problem. *J Mech Phys Solids* 46:1319–1342
62. Hofacker M, Miehe C (2012) Continuum phase field modeling of dynamic fracture: variational principles and staggered FE implementation. *Int J Fract* 178:113–129
63. Borden MJ, Verhoosel CV, Scott MA, Hughes TJR, Landis CM (2012) A phase-field description of dynamic brittle fracture. *Comp Meth Appl Mech Eng* 217–220:77–95
64. Volokh KY (2017) Fracture as a material sink. *Mater Theory* 1:3
65. Persson BNJ, Albohr O, Heinrich G, Ueba H (2005) Crack propagation in rubber-like materials. *J Phys Condens Matter* 17:R1071–R1142
66. Faye A, Lev Y, Volokh KY (2019) The effect of local inertia around the crack tip in dynamic fracture of soft materials. *Mech Soft Mater* 1:4
67. Chen CH, Bouchbinder E, Karma A (2017) Instability in dynamic fracture and the failure of the classical theory of cracks. *Nat Phys* 13:1186
68. Agrawal V, Dayal K (2017) Dependence of equilibrium Griffith surface energy on crack speed in phase-field models for fracture coupled to elastodynamics. *Int J Fract* 207:243–249